



Application of artificial accelerograms to estimating damage to dams using failure criteria

E. Zacchei* and J.L. Molina

Department of Civil Engineering, Higher Polytechnic School of Ávila, University of Salamanca (USAL), 50 Hornos Caleros Avenue, 05003, Ávila, Spain.

Received 8 April 2018; received in revised form 25 September 2018; accepted 3 December 2018

KEYWORDS

Earthquake damage estimation;
Failure modes;
Power spectral density function;
Concrete arch-dams;
Storage tanks;
Sloshing mode.

Abstract. The aim of this paper is to analyze damage to dams by using two recent methodologies. The first method was used to define the performance and response curves of concrete gravity dams. The second method defined the seismic input that was obtained from power spectral density function consistent with the response spectrum. Both methods are efficient, practical, and useful to develop quite complicated analysis as the construction of the stochastic process to define the synthetic earthquake and the estimation of cracks in the dam's body. These methodologies were explained and modified to improve their use. The fluid behavior of arch dams was compared with that of storage tanks by studying the sloshing phenomenon, which is usually neglected for dams. For the mathematical modeling, interactive programming language was used.

© 2020 Sharif University of Technology. All rights reserved.

1. Introduction

The literature offers a number of nonlinear models for estimating the response to displacements of concrete dams, all of which have yielded similar results. In this regard, we can mention some examples as follows:

- The plastic degradation method, which considers a reduction in elasto-plastic modulus during the hysteretic cycles [1,2];
- Nonlinear fracture mechanics which defines the potential crack [3];
- Modeling of the joints within the dam transmitting the interactive stresses of the blocks [4];
- The endurance time acceleration based on pushover analysis [5,6], and evaluation of the base

sliding, even though it is a simplified analysis accounting for the nonlinear behavior of the dam-water-foundation system [7].

There are also several approaches to studying the fluid-structure interaction and hydrodynamic pressures generated by water particle excitation: The Lagrangian approach which expresses fluid behavior in terms of displacements [8,9]; the Eulerian approach which expresses fluid behavior in terms of pressures [10]; and the immersed boundary methods which are based on numerical simulation [11].

The question is: “What is the most convenient model for use in terms of time and reliable results? Nowadays, scholars carry out rather complex studies that might not always turn out to be viable and applicable to engineering companies. Further to the above, the number of related software packages is surging while the need to cut down on costs and to be time efficient for engineering still remains rather unresolved.

In practice, results of structural analyses are generally compared with those of traditional methods, e.g.,

*. Corresponding author. Tel.: +34 664812367
E-mail addresses: enricozacchei@usal.es (E. Zacchei);
jlmolina@usal.es (J.L. Molina)

USACE [12]. This is because simple applications are easier to control at the expense of result accuracy. If the comparative results are backed up with specialized verification, the outcome will probably be optimal.

The agenda of recent meetings of the Committee of Large Dams (Meeting of EWG Dams and Earthquakes in Rome in February 2017 and Annual Meeting of SPANCOLD in Madrid in February 2017) was to discuss the necessity of re-analyzing and re-evaluating the existing dams so as to prevent further future damages.

In Spain, the Andalusian region (Southern Spain) is highly exposed to seismic activities [13] and a number of severe earthquakes have occurred so far; therefore, seismic analysis of the area is a necessity. Earthquake records involving arch dams are generally very limited in scope. The work described in [14] shows some of the important earthquake records of arch dams, presenting some significant remarks.

There are many methods for obtaining the seismic input, an example of which includes the probabilistic and deterministic seismic hazard assessments [15]; however, they would take some months to reach an outcome. Besides, they are usually compared with real accelerograms to identify the most consistent accelerogram for conducting the time-history dynamic analysis [16]; however, in some available database [17], it is possible to find only a short range of real accelerograms.

In this paper, two time-efficient and cost-effective methodologies were used. The first one defines the Power Spectral Density (PSD) function and the second one estimates the earthquake-induced damage to gravity dams. The first methodology is advantageous in that it provides synthetic accelerogram that allows conducting time-history dynamic analysis. In Spain, it is possible to define the synthetic accelerograms using the input data present in the Spanish code [18] by means of stochastic response [19–21]. To its advantage, the second methodology does not need to define a nonlinear model, the development and reliability of which can be quite complicated.

The final section of this paper comprises the fluid behavior of arch-dams in comparison with the fluid behavior of storage tanks. A dam-reservoir structure is a liquid storage structure of large scale [22]. The main differences between the arch-dams and tanks are as follows:

- (i) The volume of water mass contained behind the dam is greater than that in the tank;
- (ii) Closed walls and regular geometry of the tank affect the liquid in it;
- (iii) In an arch-dam which is basically a tank, the internal pressures act in different directions, whereas in the dam they always go upstream-downstream;
- (iv) The dam oscillates as a rigid monolith, whereas the (flexible) tank deforms the walls;
- (v) Tanks can be made of concrete or steel;
- (vi) In tanks, the water mass is divided into two parts: the underlying part (impulsive mass) is united rigidly with the walls, whereas the overlying part (convective mass) is united elastically with the walls and oscillates freely [23]. In addition, for storage tanks and containers [24,25], the free surface motion is known as a sloshing wave (convective mass) and is still under study, whereas it is usually neglected for dams.

2. Case study

To estimate the damage imposed on dams and the sloshing mode, two types of dams were considered in this study. The dams are located in the Andalusian region (Southern Spain) with high susceptibility to relative seismic hazard. The studied seismogenic zone where both dams are placed is ZS34 [26], the characterization of which is given as follows: The tectonic dominant mechanism is reverse fault, the mean maximum moment magnitude (M_w) is 6.6 ± 0.3 , and the mean annual rate of exceedance for $M_w \geq 4.0$ is 0.198 (≈ 5 years, i.e., the mean time interval between occurrences of events). In accordance to [27], the two dams (see Figure 1) were considered large because they satisfied the following condition: $h = \{89.55 \text{ m}, 74.0 \text{ m}\} > 15 \text{ m}$ and $c_r = \{57.0 \text{ hm}^3, 84.0 \text{ hm}^3\} > 1 \text{ hm}^3$. The numbers in the brackets represent the Concepción Dam and Conde de Guadalhorce Dam, respectively. The parameter c_r is the reservoir capacity and h is the maximum height of the dam. Table 1 shows a description of the data.

3. Materials and methods

3.1. Definition of artificial accelerograms

There are some codes that help calculate the elastic spectrum using curves with three or four branches. In this case, for the last branch, the circular frequency ω tends to infinity. For example, the Brazilian [28], Spanish [18], and Venezuelan [29] codes use three branches, whereas the Italian [30] and European [31] codes use four branches. The lack of the last fourth branch could not be much significant, because in the flexible structures (with long periods), the accelerations are not transmitted totally to the structure. Consequently, an underestimated pseudo-static force is not much relevant. Usually, the codes with four branches have the fourth branch as the lowest one.

In this section, the definition of artificial accelerograms is carried out using a methodology that would

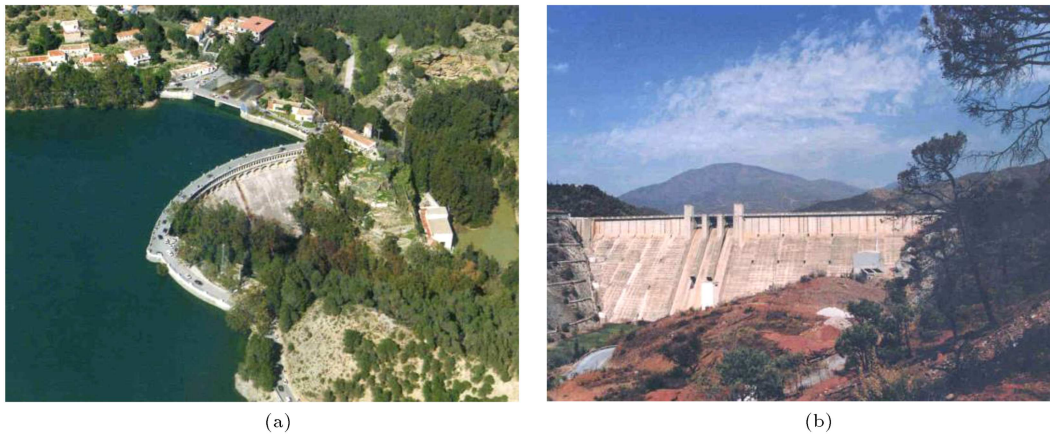


Figure 1. (a) The Conde de Guadalhorce Dam and (b) Concepción Dam.

Table 1. Description of the data.

	La Concepción Dam	Conde de Guadalhorce Dam
Type of dam	Gravity	Arch gravity
Year of construction	1971	1921
Crown length (m)	256	160
Crown width (m)	6.5	6.0
Downstream slope	1:0.75	1:0.89
Upstream slope	1:0.05	1:0.03
Dam volume (m ³)	519000	137000
Height (m)	89.55	74.00
Estimated radius (m)	—	140.0
Reservoir area (ha) ^a	214	546
Reservoir capacity c_r (hm ³)	57.0	84.0
Basin area (km ²)	142	271
Water level (m)	103.175 ± 3.675	343.3 ± 0.8
Spillway capacity (m ³ /s)	580	606
River	Verde	Ardales/Turón
Province	Malaga	Malaga
Seismogenic zone	ZS34	ZS34

^a: The area of the reservoir is calculated for the maximum operating level.

be applicable to the Spanish elastic spectrum [18] with three branches.

The methodology developed by Barone et al. (2015) [32] is elaborated in the following (see Figure 2). First, the elastic spectrum parameters were chosen: T_A , T_B , ω_A , ω_B , Peak Ground Acceleration (PGA), and viscous damping ratio, ξ . Then, Peak Factor (PF) was expressed by Eq. (2) and the parameters that help obtain the PSD function expressed by Eq. (1) were determined. PF was the maximum probable value of response and was equivalent to the displacement obtained by pseudo-acceleration spectral response times the circular frequency squared.

After that, the deterministic modulation function $I(t)$ and the amplitude of the accelerogram $A_i \approx$

$\sqrt{2PSD(\omega_i)\Delta\omega_i}$ [33] were calculated. Finally, the artificial accelerograms were computed.

In this analysis, being a stochastic approach, it is possible that the artificial accelerogram would have some inconsistencies, e.g., the difference between the maximum acceleration of the artificial accelerogram and the PGA cannot be significant (see Figure 3(b)), or the final velocity, obtained as an integrate of the artificial acceleration, cannot be null. The former is solved by scaling all values of the artificial accelerogram. Herein, the maximum scale factor is 2.72(= 0.924/0.34) higher than the input PGA (despite this, it has not been scaled in the current analysis because the focus here is to create cracks – this also justifies the use of the overestimated soil amplification). The latter is solved

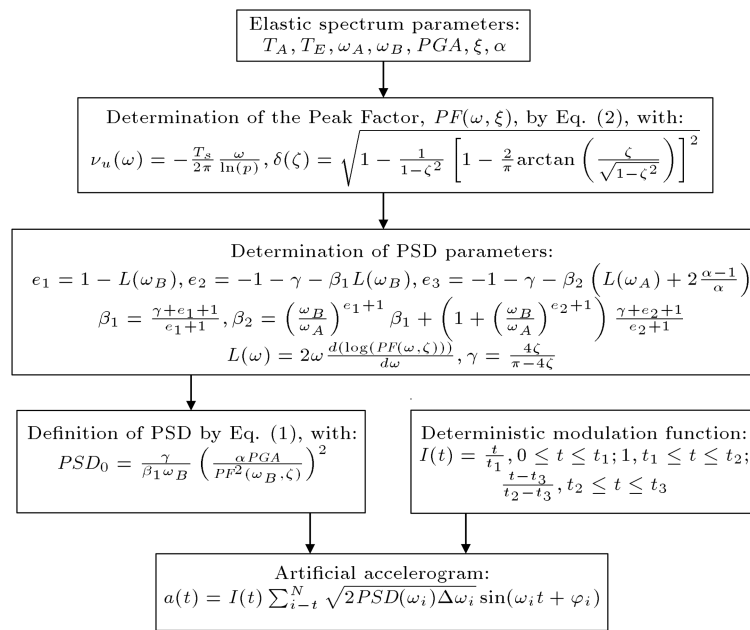


Figure 2. Flow chart of the definition of artificial accelerogram.

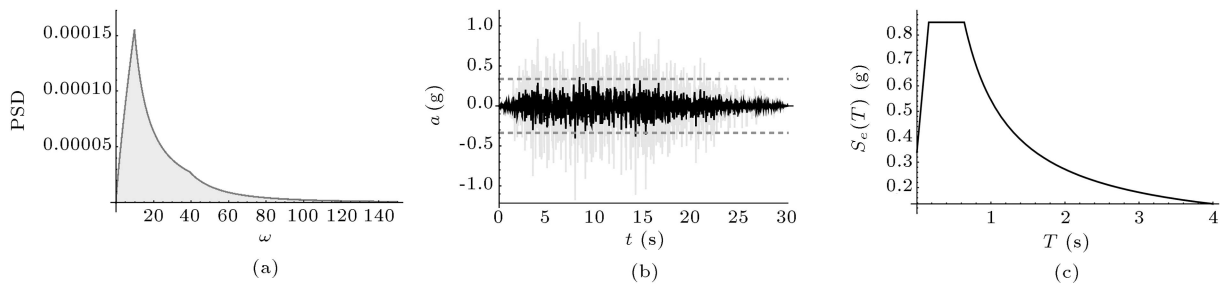


Figure 3. (a) Power Spectral Density (PSD), (b) artificial accelerations, and (c) and elastic spectrum. The horizontal dashed lines in (b) refer to $PGA = 0.34$ g.

using the baseline correction. This correction induces important changes in the ground displacement and in the velocity diagrams; however, in the accelerations, there are no noticeable alterations [34], thus, the baseline correction has been neglected.

However, the applied analytical model defines the PSD function coherent with response spectrum; thus, the aspect that must be respected must be the distribution of power (amount of energy transferred per unit time) versus the frequency.

The used acceleration value represents the higher value shown in the Spanish code [18] in the Malaga province, which is 0.21 g. The PGA was calculated considering the structures as special (coefficient equal to 1.3) and the soil amplification as III/IV-type (soil coefficient ~ 1.8 and ground amplification coefficient ~ 1.25). Much of the Southern Spain soil is of types I(A), I(B), and II; however, there are also areas of type III/IV(A)- [13]. The calculated PGA is equal to 0.34 g ($= 0.21 \text{ g} \times 1.3 \times 1.25$).

The dynamic amplification factor α is 2.5 and the natural (service life) periods of the structure are:

$T_A = 0.16$ s ($\omega_A = 39.269$ rad/s) and $T_B = 0.64$ s ($\omega_B = 9.817$ rad/s). To define the structural periods, the contribution coefficient K , which is considered in the three-branches expression in the Spanish code [18], is neglected. In the Spanish code [18], K is listed for each city and ranges between 1.0–1.3. It accounts for the seismic hazard; however, given that there are many unknown parameters that represent the complexity of defining the seismic hazard [35,36], the authors believe that K has no meaning.

The PSD by Barone et al. (2015) [32] is defined as follows:

$$\begin{cases} PSD_0 \left(\frac{\omega}{\omega_B}\right)^{e_1} & \text{for } 0 < \omega \leq \omega_B \\ PSD_0 \left(\frac{\omega}{\omega_B}\right)^{e_2} & \text{for } \omega_B < \omega \leq \omega_A \\ PSD_0 \left(\frac{\omega_A}{\omega_B}\right)^{e_2} \left(\frac{\omega}{\omega_A}\right)^{e_3} & \text{for } \omega > \omega_A \end{cases} \quad (1)$$

where $PSD_0 = 1.554 \times 10^{-4} \text{ g}^2/(\text{rad/s})$ is the peak value of the PSD function at a frequency of $\omega = \omega_B$.

These three equations depend on ω , PF, ξ , and α . In this analysis, the three exponentials are: $e_1 = 0.826$, $e_2 = -1.247$, and $e_3 = -2.592$. The PF [37] is defined as follows:

$$PF(\omega, \xi) = \sqrt{2In \left[2\nu_u \left(1 - e^{-\delta^{1.2} \sqrt{\pi In(2\nu_u)}} \right) \right]}, \quad (2)$$

where the parameter ν_u ($\nu_u = 17.146$, when $\omega = \omega_B$; $\nu_u = 68.585$, when $\omega = \omega_A$) depends on nominal duration T_s of the pseudo-stationary part and probability function p . The probability function p was assumed equal to 0.367, i.e., the mean value of the peak values could be approximated by the 36.7% fractile of the maximum distribution. The parameter $\delta = 0.245$ is called “spread factor” and correlates with $\xi = 0.05$. The nominal duration was assumed $T_s = 11$ s. The choice of the nominal duration value can be assumed in accordance with the significant duration, as shown in the previous work [36,38].

The earthquake motion is defined by a non-stationary process and the nonlinear dynamic response of the structures is highly influenced by the non-stationary behavior of the seismic input; the earthquakes are usually too short in duration to let the response become stationary. However, in this study, the central time interval was assumed stationary and the end and initial time intervals were assumed as non-stationary to preserve the increasing and decreasing trends of the accelerogram in the initial and final phases, respectively.

To simulate the quasi-stationary condition of the real earthquakes, it is necessary to define the deterministic modulating function; to this end, the trapezoidal shape was chosen [39]; the three branches were 0–4 s, 4–15 s, and 15–30 s, where $t_1 = 4$ s, $t_2 = t_1 + T_s = 4$ s + 11 s = 15 s, and $t_3 = 30$ s.

Finally, to define $a(t)$, the number of the used harmonic waves (superposition method) with random phases (φ_i) by Preumont [34] is: $N \geq (150/\pi)t_3 = (150/\pi)30 = 1432 \rightarrow 1500$, where 150 rad/s is the cut-off circular frequency selected.

Figure 3 shows the PSD in function of ω , the artificial accelerogram a (g) in the time domain t (s), and the elastic spectrum (spectral accelerations S_e versus structural periods T).

The shape of the PSD is similar to that of other ones in the literature [40,41]. PSD is not slope-wise continuous at the control frequencies; this may be attributed to the slope discontinuities at these frequencies in the response spectrum [42].

3.2. Estimation of earthquake damage

The estimation of earthquake-induced damage to gravity dams was performed using the methodology proposed by Alembagheri (2016) [43]. The method is

composed of calculating the Performance Curve (P-C) and the Response Curve (R-C) of dams.

In Alembagheri’s work (2016) [43], the pushover curve was used to define the yielding and ultimate displacements; instead, in this analysis, the pushover curve was estimated. This is because the dam body was subjected to increase in the tensile stresses, as required by the standards of pushover analysis. Given that the concrete tensile capacity was weak, we expect poor results. Moreover, the pushover analysis is usually used for new constructions.

The flow chart in Figure 4 shows the methodology of estimating the P-C and R-C as well as the Damage Index (DI) of concrete gravity dams. The procedure of the flow chart is elaborated in the following.

To define the Cumulative Inelastic Area (CIA) of the P-C, the process is divided into:

- (i) Estimation of C_u , C_y and definition of T_1 in the trigonometric function (3);
- (ii) Quantification of the number of Demand-Capacity Ratio (DCR);
- (iii) Calculation of the CIA of the P-C curve;
- (iv) Drawing of the curves P-C, 2P-C (two times P-C curve), and 3P-C (three times P-C curve).

The area is between $(C_u/C_y)_i$ of step i and $(C_u/C_y)_{\max}$; in this analysis, seven points ($i = 7$) were used (for more details, see Figure 3 in [43]).

Because the first vibration mode of the gravity dams is predominant and each block can be considered as a simple oscillator, DCR can be assumed as a Harmonic Crest Displacement (CDH) time-history with the following equation:

$$CDH = \frac{C_u}{C_y} \sin \frac{2\pi t}{T_1}, \quad (3)$$

where C_u and C_y are the ultimate and yielding crest displacement capacities and T_1 is the dam fundamental period.

Defining the R-C, the process is similar to the process employed to calculate P-C, because, due to the considerable irregularity of the earthquake accelerations, CIA is too complicated to calculate.

To solve this problem, the following approximation was used:

$$CIA = (2 \times 0.05) \times n_p / (2 \times 3) = 0.1(n_p/6).$$

The process comprised:

- (i) Defining the C_y ;
- (ii) Individualizing the sum of the elastic displacement peaks n_p that exceed C_{yi} ;
- (iii) Multiplying n_p by two times the step time $d_t = 0.05$ s.

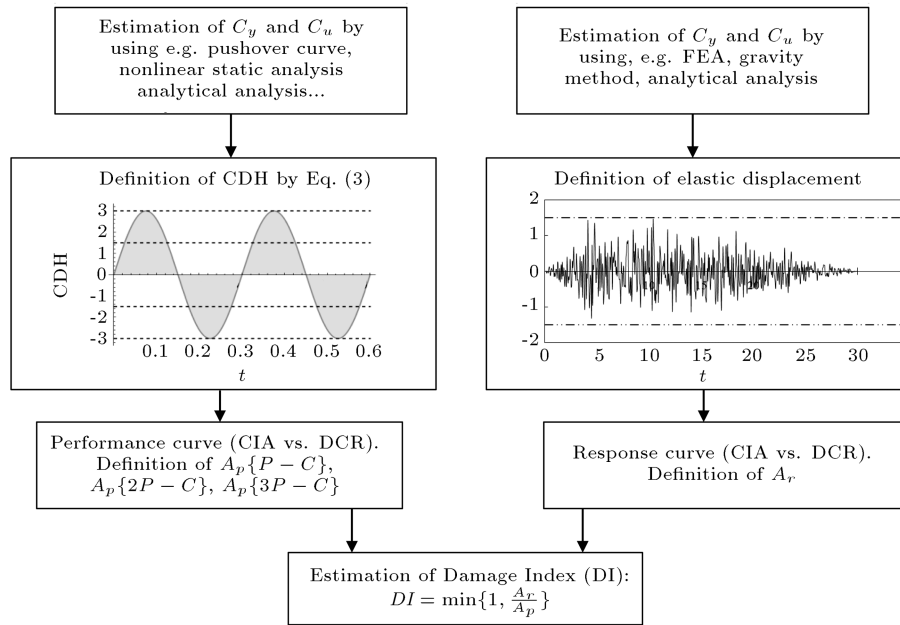


Figure 4. Flow chart of the estimation of the damage index.

To eliminate the descending branches of the time-history and to consider only the positive peak times, the division by two and three was made, respectively. The displacement occurred between C_{yi} of step i and $C_{y,max}$, where seven points ($i = 7$) were used. DCR ranges between 1.0 and the maximum elastic displacement divided by C_y (for more details, see Figure 1 in [43]).

Table 2 shows the data of the dam block for the analysis. The objective here is to study the response of the individual block idealized as a triangular shape (fundamental triangle) by considering different structural periods and different C_u/C_y ratios. The structural periods were considered in a common range of 0.25–0.35 s for dams, whereas C_u/C_y ratio ranged

Table 2. Data concerning central block (fundamental triangle) of the Concepción Dam.

Height (m)	77.50
Base (m)	62.00
Volume (m ³)	2402.50
Mass density of concrete (kN/m ³)	24.0
Mass (10 ³ kg)	5766.0
	0.25
T_1 (s)	0.30
	0.35
	3642.12
Stiffness (MN/m) ^a	2529.25
	1858.22

^a: The stiffness is obtained by equation $T_1 = 2\pi(\text{mass}/\text{stiffness})^{1/2}$.

between 1.5–4.0, which were the same values calculated in the literature [43]. The value of C_y was fixed at 1.50 cm. The literature provides a glimpse of the three types of concrete gravity dams [43] like the Concepción Dam, thus attesting the reliability of the data.

4. Results of the damage estimation

To estimate the P-C and R-C, an analytical analysis was conducted and the dam-water-foundation interaction was not considered. However, it needs to be mentioned that by considering dam-water-foundation interaction, the structural period increases to 0.65 s [44].

Figure 5 shows the CDH in the time domain of the studied dam for $T_1 = 0.3$ s. The horizontal dashed lines correspond to $C_u/C_y = 3$ and $C_y = 1.5$ cm. Figure 6 shows the elastic displacement in the time domain and the yielding crest displacement C_y for $T_1 = 0.3$ s. The elastic displacement was calculated by (mass x

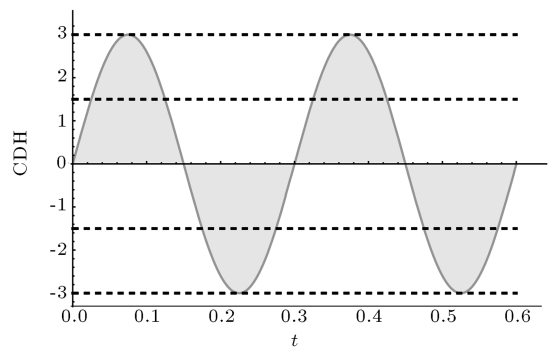


Figure 5. Harmonic Crest Displacement (CDH) in the time domain of the Concepción Dam for $C_u/C_y = 3$, $C_y = 1.5$ cm, and $T_1 = 0.3$ s.

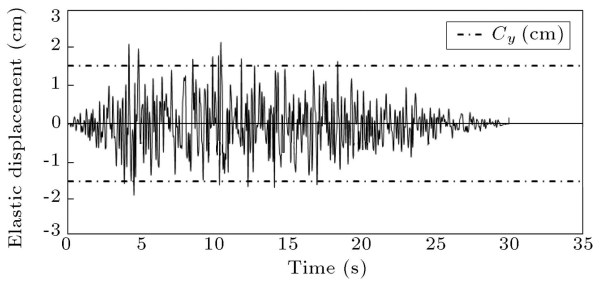


Figure 6. Elastic displacement of the La Concepción Dam for $C_u/C_y = 3$, $C_y = 1.5$ cm and $T_1 = 0.3$ s ($n_p = 31$).

acceleration)/stiffness. n_p indicates the number of times that the elastic displacement exceeds C_{yi} .

Table 3 shows the area under the P-C, two times P-C, and three times P-C of the Concepción Dam. The parameters \bar{y}_{CIA} and \bar{x}_{DCR} are the mean values of the CIA and DCR, considering the seven points that draw the P-C and R-C.

Figures 7–9 show P-C (dashed line) and R-C (solid line) for the Concepción Dam. The highest R-C and the highest P-C represent the R-C calculated by $a(g)$ and the 3P-C curve, respectively.

After defining the P-C and R-C, it is possible to define the DI by $\min(1, A_r/A_p)$, where A_p is the area under 2P-C (see underlined values in Table 3) and A_r is the area under R-C (see underlined values in Table 4). If $DI \leq 0.5$, the dam essentially remains intact or suffers minor damage; if $0.5 < DI < 1.0$, the dam damage is moderate or operational; and if $DI = 1.0$, the dam is subject to severe damage.

The damages of the dam body usually occur in the base (heel and toe), in the crown, and in the points where the slopes change. The cracks can propagate along the whole upstream and downstream face, as shown in literature [45–47].

5. Sloshing modes

An arch-dam can be considered to be part of a tank

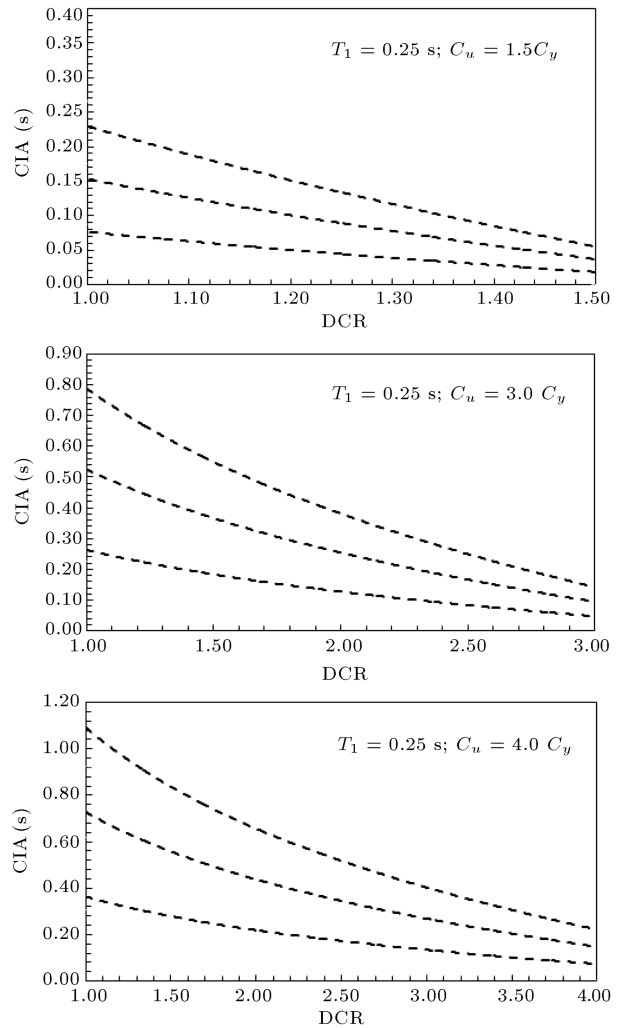


Figure 7. Analysis results of the Concepción Dam for $T_1 = 0.25$ s. The performance curves are indicated by the dashed lines and the response curves by solid lines.

circumference [48]. In this analysis, the dam idealized as a tank is the Conde de Guadalhorce Dam.

The parametric equations for the equivalent tank with the reduced radius (Figure 10(a)) and the tank

Table 3. Performance curve data of the La Concepción Dam.

T_1 (s)	C_u/C_y	P-C			2P-C			3P-C		
		A_p	\bar{y}_{CIA} (s)	\bar{x}_{DCR}	A_p	\bar{y}_{CIA} (s)	\bar{x}_{DCR}	A_p	\bar{y}_{CIA} (s)	\bar{x}_{DCR}
0.25	1.5	0.378	0.054	1.205	0.756	0.108	1.205	1.134	0.162	1.205
	3.0	0.808	0.115	2.268	1.616	0.230	2.268	2.424	0.345	2.268
	4.0	1.086	0.155	2.977	2.172	0.310	2.977	3.258	0.465	2.977
0.30	1.5	0.546	0.078	1.124	1.092	0.156	1.124	1.638	0.234	1.124
	3.0	1.156	0.165	2.106	2.312	0.330	2.106	3.468	0.495	2.106
	4.0	1.550	0.221	2.761	3.10	0.442	2.761	4.650	0.663	2.761
0.35	1.5	0.717	0.102	1.048	1.434	0.204	1.048	2.151	0.306	1.048
	3.0	1.503	0.215	1.953	3.006	0.430	1.953	4.509	0.645	1.953
	4.0	2.017	0.288	2.556	4.034	0.576	2.556	6.051	0.864	2.556

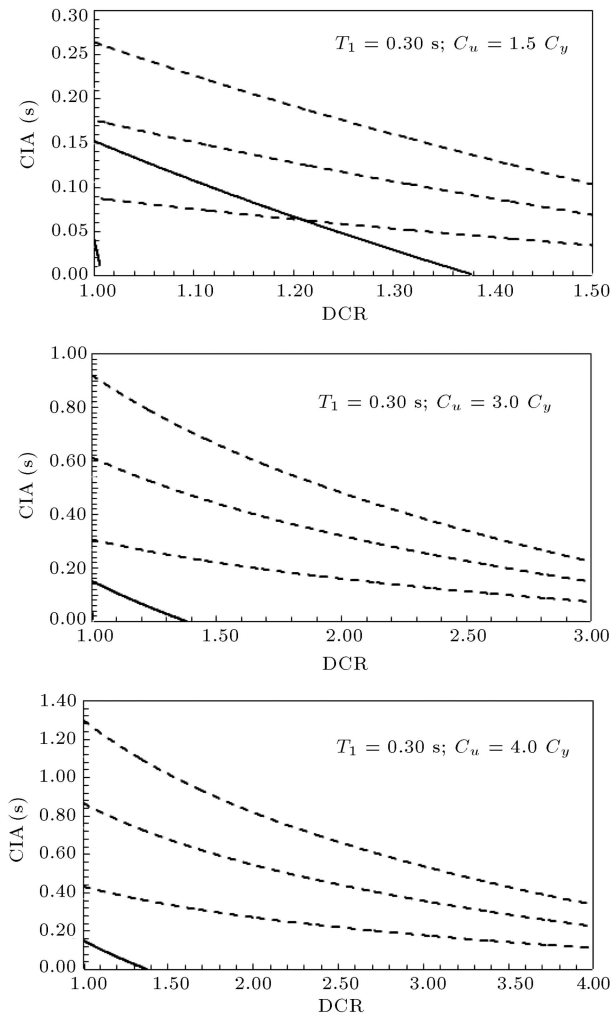


Figure 8. Analysis results of the Concepción Dam for $T_1 = 0.30$ s. The performance curves are indicated by the dashed lines and the response curves by solid lines.

with the estimated radius (140 m) (Figure 10(b)) are $\{\cos(r), \sin(r), z|0 < r < 2\pi, 0 < z < 1.143\}$ and $\{\cos(r), \sin(r), z|0 < r < 2\pi, 0 < z < 0.375\}$, respectively, where z is the vertical axis and r is the radius coordinate.

The height of the equivalent tank was scaled at 1 : 10 in relation to the fundamental triangle height of the dam which is 52.5 m ($\rightarrow H_{tank} = 5.25$ m), whereas the radius is less than 30.5 times the estimated radius of the dam ($\rightarrow R = 4.59$ m). The criterion used to define the tank radius relies on considering at least 7/8 of the liquid height H by us Army Corps of Engineers [49]:

$$p_w = 7/8\rho PGA[1 - (z/H)]^{1/2},$$

where $\rho = 1000$ kg/m³ (mass density of the water). Therefore, $R \rightarrow (7/8) \times 5.25 = 4.59$ m.

The impulsive p_i and sloshing p_c [50] pressures for the first mode were computed through the following equations:

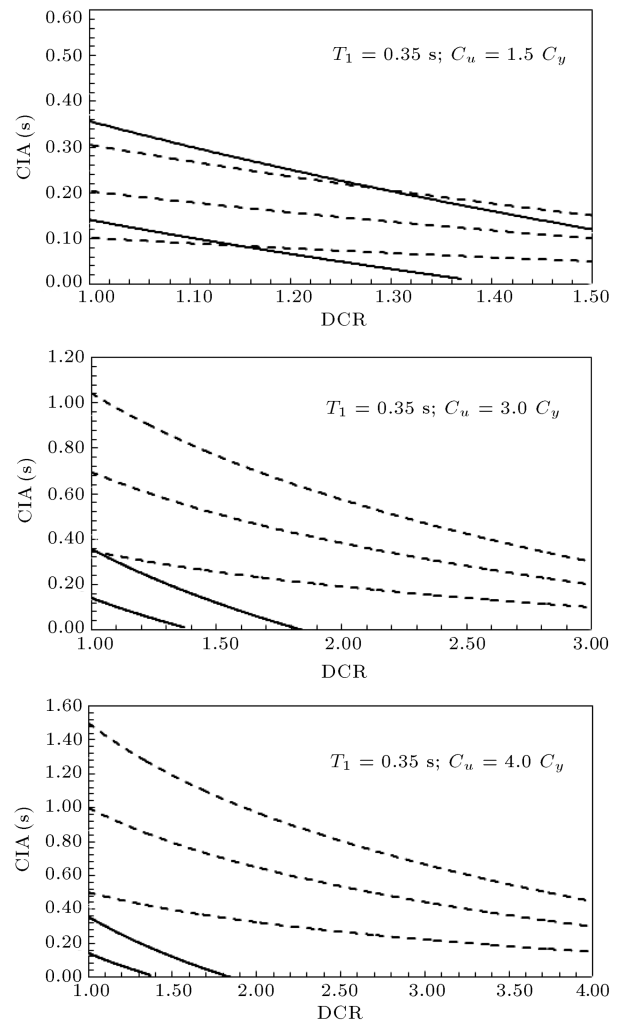


Figure 9. Analysis results of the Concepción Dam for $T_1 = 0.35$ s. The performance curves are indicated by the dashed lines and the response curves by solid lines.

$$\frac{p_i\left(\frac{z}{H}, t\right)}{PGA} = \frac{2\rho H}{\left[I_0\left(\frac{\nu_0 R}{H}\right) - \left(\frac{H}{\nu_0 R}\right)\left(I_1\left(\frac{\nu_0 R}{H}\right)\right)\right]v_0^2} \cos\left(\frac{\nu_0 z}{H}\right) I_1\left(\frac{\nu_0 R}{H}\right), \quad (4)$$

$$\frac{p_c\left(\frac{z}{H}, t\right)}{PSA} = \frac{2\rho H}{(\lambda_1^2 - 1) J_1(\lambda_1) \cosh\left(\frac{\lambda_1 H}{R}\right)} \cos\left(\frac{\lambda_1 z}{R}\right) J_1(\lambda_1), \quad (5)$$

where $\nu_0 = 1.5707$, $I_1 = 1.0538$, and $I_0 = 1.7187$ correspond to the modified Bessel function of order one and zero, respectively, and $J_1 = 0.5818$ is the Bessel function of the order one. Pseudo Spectra Acceleration (PSA) was calculated considering the sloshing circular frequency, $\omega_{cn} (= 2\pi/T_{cn})$ by:

$$\omega_{cn} = [(g\lambda_n/R) \tanh(\lambda_n H/R)]^{1/2},$$

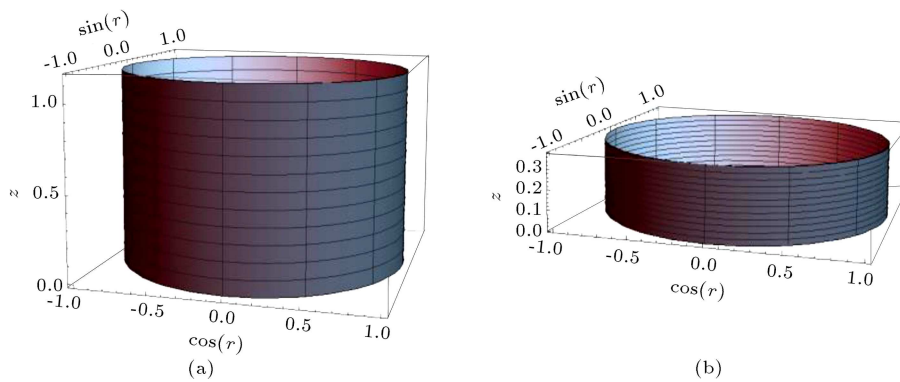


Figure 10. Geometrical model of the equivalent tank with $R = 4.59$ m, 144 meshes of 0.095×0.523 m (a), and tank with $R = 140$ m, 144 meshes of 0.031×0.523 m (b) by software [52].

Table 4. Response curve results of the La Concepción Dam.

T_1 (s)	C_u/C_y	$a(g)$				$a(g)/1.37$				$a(g)/2.74$			
		A_r	\bar{y}_{CIA} (s)	\bar{x}_{DCR}	DI	A_r	\bar{y}_{CIA} (s)	\bar{x}_{DCR}	DI	A_r	\bar{y}_{CIA} (s)	\bar{x}_{DCR}	DI
0.25	1.5				0.0				0.0				0.0
	3.0	<u>0.0</u>	0.0	0.978	0.0	<u>0.0</u>	0.0	0.849	0.0	<u>0.0</u>	0.0	0.675	0.0
	4.0				0.0				0.0				0.0
0.30	1.5				0.473				0.168				0.0
	3.0	<u>0.517</u>	0.074	1.189	0.224	<u>0.183</u>	0.026	1.003	0.079	<u>0.0</u>	0.0	0.751	0.0
	4.0				0.167				0.059				0.0
0.35	1.5				0.767				0.360				0.0
	3.0	<u>1.10</u>	0.157	1.438	0.366	<u>0.517</u>	0.074	1.184	0.172	<u>0.0</u>	0.0	0.842	0.0
	4.0				0.273				0.128				0.0

where $\lambda_n = \{1.841, 5.331, 8.536\}$ and $n = \{1, 2, 3\}$ for the first three modes; and g is the gravity. All pressures were calculated at the wall of the tank and on the plane of the horizontal seismic action.

For $H = R = 4.59$ m, the ω_{cn} for the first three modes is 1.934 rad/s ($T_{c1} = 3.248$ s), 3.376 rad/s ($T_{c2} = 1.861$ s), and 4.271 rad/s ($T_{c3} = 1.471$ s). Considering $H = 42$ m and $R = 140$ m, $T_{c1} = 24.73$ s ($\omega_{c1} = 0.254$ rad/s).

PSA, for the soil coefficient equal to 2, is 0.21 g ($= 0.34 \text{ g} \times (2/3.248)$) [18]. The final PSA is 0.28 g ($= 0.21 \text{ g} \times 1.348$), where the damping factor is defined by $[10/(5 + \xi)]^{1/2} = 1.348$ for $\xi = 0.5\%$ [31].

Table 5 shows the pressure results and Table 6 shows the summary of the data. The peak sloshing wave is [51]:

$$d_{\max} = 0.84 \times R \times (PSA/g) = 0.84 \times 4.59 \times 0.28 = 1.08 \text{ m.}$$

6. Conclusion

This paper described two methodologies for defining artificial acceleration using a novel analytical model of Power Spectral Density (PSD) and estimated the damage to concrete gravity dams. The main advantage

of the first methodology was that it could be highly applicable to and compatible with different spectra, whereas the main advantage of the second one was that it did not need a nonlinear model to define the material behavior.

Two large dams in the region of Southern Spain – built between the years 1921 and 1971 – were analyzed here because, in this region, the seismic hazard was intense (the greatest recorded magnitude was $M_w 6.9$).

The first dam, Concepción Dam, was studied to estimate the damage index under the artificial acceleration consistent with Spanish elastic spectrum. The stochastic analysis used to define the artificial acceleration was based on the assumptions that the time-history earthquake, necessary to do the dynamic analysis, was a realization of random processes. The obtained maximum value was 0.977 g. Because the first vibration mode of the gravity dams was predominant, the damage analysis was based on the fact that the cumulative inelastic area could be assumed as a harmonic crest displacement time-history. The obtained damage index ranged from 0 to 0.767, i.e., when the dam was intact and when it was moderately damaged.

Finally, the second dam, Conde de Guadalhorce Dam, was compared to the storage tank to study the

Table 5. Dynamic pressures (the unit is kN/m²).

z/H	Equivalent tank			Arch-dam	
	p_i	p_c	$p_i + p_c$	p_w	$p_w - p_i$
1.00	0	10.554	10.54	0	0
0.50	8.747	4.751	13.498	9.631	0.884
0.00	12.370	3.267	15.637	13.275	0.905
Mean pressure ^a	7.231	5.887	13.117	8.177	0.946
Mean force ^a	25.551 ^b	26.643 ^c	32.298 ^b	27.420 ^b	—

^a: The mean values were calculated considering the points of their resulting acts, i.e., between $0.4H$ and $0.6H$;

^b: This value was calculated considering the mean between $0.5 \times H \times p_{\max}$ and $0.4 \times H \times p_{\max}$;

^c: This value was calculated considering the mean between $0.6 \times H \times p_{\max}$ and $0.5 \times H \times p_{\max}$.

Table 6. Summary of the data.

	R (m)	H_{tank} (m)	H (m)	T_{c1} (s) ^a	m_c (kg)	ξ_c (%)	$PSA _{\xi_c=5.0\%}$ (g) ^b	$PSA _{\xi_c=0.5\%}$ (g) ^b	d_{\max} (m)	$x(t)$ (m) ^c
Equivalent tank	4.59	5.25	4.59	3.248	137×10^3	0.5	0.21	0.28	1.08	0.75
Tank	140.0	52.5	42.0	24.73	2.13×10^6	0.5	0.21	0.28	—	43.40

^a: Sloshing period of the first mode;

^b: The elastic spectrum was calculated with a viscous damping ratio of 5% for concrete and 0.5% for liquid;

^c: The sloshing displacement $x(t)$ as a continuum was calculated by the equation of motion [53].

sloshing effect. Both systems exhibited some differences, while they shared some similarities. A dam-reservoir system may become a large-scale storage-tank system. The mean value of the difference between the dynamic pressures of the dam and those of the equivalent tank was 0.946 kN/m². For the equivalent tank, the first sloshing frequency was 0.307 Hz and the height of the waves reached 1.08 m.

Acknowledgement

The first author acknowledges the “Servicios Informáticos CPD” of the University of Salamanca for the Wolfram Mathematica license and the University of Salamanca to pay the rights (when applicable) to completely download all papers in the references.

References

1. Omidi, O. and Lotfi, V. “Seismic plastic-damage analysis of mass concrete blocks in arch dams including contraction and peripheral joints”, *Soil Dyn. Earth. Eng.*, **95**, pp. 118–137 (2017).
2. Lubliner, J., Oliver, J., Oller, S., et al. “A plastic-damage model for concrete”, *Int. J. Sol. Struc.*, **25**(3), pp. 299–326 (1989).
3. Guanglun, W., Pekau, O.A., Chuhan, Z., et al. “Seismic fracture analysis of concrete gravity dams based

on nonlinear fracture mechanics”, *Eng. Frac. Mech.*, **65**, pp. 67–87 (2000).

4. Wang, J.T., Jin, A.Y., Du, X.L., et al. “Scatter of dynamic response and damage of an arch dam subjected to artificial earthquake accelerograms”, *Soil Dyn. Earth. Eng.*, **87**, pp. 93–100 (2016).
5. Hariri-Ardebili, M.A., Furgani, L., Meghella, M., et al. “A new class of seismic damage and performance indices for arch dams via ETA method”, *Eng. Struc.*, **110**, pp. 145–160 (2016).
6. Hariri-Ardebili, M.A., Mirzabozorg, H., and Kianoush, R. “Comparative study of endurance time and time history methods in seismic analysis of high arch dams”, *Inter. J. Civ. Eng.*, **12**(2), pp. 219–236 (2014).
7. Basili, M. and Nuti, C. “A simplified procedure for base sliding evaluation of concrete gravity dams under seismic action”, *Inter. Schol. Resea. Netw.*, **2011**, pp. 1–14 (2011).
8. Akköse, M., Adanur, S., Bayraktar, A., et al. “Elasto-plastic earthquake response of arch dams including fluid-structure interaction by the Lagrangian approach”, *App. Math. Mod.*, **32**, pp. 2396–2412 (2008).
9. Amina, T.B., Mohamed, B., André, L., et al. “Fluid-structure interaction of Brezina arch dam: 3D modal analysis”, *Eng. Struc.*, **84**, pp. 19–28 (2015).
10. Khosravi, S. and Mohammad, M.H. “Modelling of concrete gravity dam including dam-water-foundation rock interaction”, *World App. Scie. J.*, **22**(4), pp. 538–546 (2013).

11. Demirel, E. “Numerical simulation of earthquake excited dam-reservoirs with irregular geometrics using an immersed boundary method”, *Soil Dyn. Earth. Eng.*, **73**, pp. 80–90 (2015).
12. U.S. Army Corps of Engineers (USACE) “Arch dam design”, Engineer Manual 1110-2-2201, Washington, District of Columbia, United States (1994).
13. Benito, M.B., Navarro, M., Vidal, F., et al. “A new seismic hazard assessment in the region of Andalusia (Southern Spain)”, *Bull. Earth. Eng.*, **8**, pp. 739–766 (2010).
14. Yang, J., Jin, F., Wang, J.T., et al. “System identification and modal analysis of an arch dam based on earthquake response records”, *Soil Dyn. Earth. Eng.*, **92**, pp. 109–121 (2017).
15. Garcia-Mayordomo, J. and Insua-Arévalo, J.M. “Seismic hazard assessment for the Itoiz dam site (Western Pyrenees, Spain)”, *Soil Dyn. Earth. Eng.*, **31**, pp. 1051–1063 (2011).
16. Bommer, J.J. and Acevedo, A.B. “The use of real earthquake accelerograms as input to dynamic analysis”, *J. Earth. Eng.*, **8**, pp. 43–91 (2004).
17. Engineering Strong-Motion database (ESM), esm.mi.ingv.it/
18. Permanent Commission on Earthquake Resistant Standards (NCSE), “Earthquake-resistant construction standard - General part and construction”, Madrid, Spain (2002).
19. Barbato, M. and Conte, J.P. “Spectral characteristics of non-stationary random processes: Theory and applications to linear structural models”, *Prob. Eng. Mech.*, **23**, pp. 416–426 (2008).
20. Koutsourelakis, P.S. “A note on the first-passage problem and VanMarcke’s approximation - short communication”, *Prob. Eng. Mech.*, **22**, pp. 22–26 (2007).
21. Bilici, Y., Bayraktar, A., Soyuluk, K., et al. “Stochastic dynamic response of dam-reservoir-foundation systems to spatially varying earthquake ground motions”, *Soil Dyn. Earth. Eng.*, **29**, pp. 444–458 (2009).
22. Koh, H.M., Kim, J.K., and Park, J.H. “Fluid-structure interaction analysis of 3-D rectangular tanks by a variationally coupled BEM-FEM and comparison with test results”, *Earth Eng. Stru. Dyn.*, **27**, pp. 109–124 (1998).
23. Housner, G.W. “The dynamic behavior of water tanks”, *Bull. Seism. Soc. Am.*, **53**(2), pp. 381–387 (1963).
24. Zheng, X., Ma, Q.W., and Duan, W.Y. “Comparison of different iterative schemes for ISPH based on Rankine source solution”, *Int. J. Nav. Arch. Oce. Eng.*, **9**, pp. 390–403 (2017).
25. Qin, J., Chen, B., and Lu, L. “Finite element based viscous numerical wave flume”, *Adv. Mech. Eng.*, **2013**, pp. 1–17 (2013).
26. Seismogenic Source Zones of the Iberian Peninsula (ZESIS) (2015). <http://info.igme.es/zesis>
27. International Commission on Large Dams (ICOLD), “Selecting seismic parameters for large dams”, Bulletin No. 148, Paris, France (2016).
28. Brazilian Association of Technical Standards (ABNT) “Project of earthquake resistant structures - Procedure”, ABNT NBR 15421:2006, Rio de Janeiro, Brazil (2006).
29. Venezuelan Foundation for Seismological Research (FUNVISIS) “Earthquake-resistant buildings - Part 1: Requirements”, COVENIN 1756-1:2001, Caracas, Venezuela (2001).
30. Ministry of Infrastructure and Transport (MIT) “Technical standards for buildings”, NTR 2008, Roma, Italy (2008).
31. Comité Européen de Normalisation (CEN) “Design of structures for earthquake resistance - Part 1: General rules, seismic actions and rules for buildings”, EN 1998-1:2004, Brussels, Belgium (2004).
32. Barone, G., Lo Iacono F., Navarra, G., et al. “A novel analytical model of power spectral density function coherent with earthquake response spectra”, *1st EC-COMAS Them. Conf. Unc. Quant. Comp. Sci. Eng. UNCECOMP 2015*, Crete Island, Greece, pp. 1–13 (2015).
33. Barbat, A.H., Orosco, L., Hurtado, J.E., et al., *Definition of Seismic Action*, International Center for Numerical Methods in Engineering, Seismic Engineering Monographs, Monograph CIMNE IS-10 (1994).
34. Preumont, A. “The generation of spectrum compatible accelerograms for the design of nuclear power plants”, *Earth. Eng. Stru. Dyn.*, **12**, pp. 481–497 (1984).
35. Fergany, E. and Hutchings, L. “Demonstration of pb-PSHA with Ras-Elhekma earthquake, Egypt”, *NRIAG J. Astr. Geoph.*, **6**(1), pp. 41–51 (2017).
36. Zacchei, E., Molina, J.L., and Brasil, L.R.F.R.M. “Seismic hazard assessment of arch dams via dynamicmodelling: an application to the Rules Dam in Granada, SE Spain”, *Int. J. Civ. Eng.*, **2017**, pp. 1–10 (2017).
37. Cacciola, P. “A stochastic approach for generating spectrum compatible fully nonstationary earthquakes”, *Comp. Stru.*, **88**(15), pp. 889–901 (2010).
38. Der Kiureghian, A. “A response spectrum method for random vibrations”, Earthquake Engineering Research Center, Report No. UCB/EERC-80/15, Berkeley, California (1980).
39. Chtcot, R. and Brasil, L.R.F.M.R. “Seismic analysis of a shear building model”, *Proc. XXXVII Ibe. Latin-Ame. Congr. Comp. Meth. Eng. CILAMCE 2016*, Brasilia, Brazil, pp. 1–12 (2016).
40. Cottone, G. and Di Paola, M. “A new representation of power spectral density and correlation function by means of fractional spectral moments”, *Prob. Eng. Mech.*, **25**, pp. 348–353 (2010).
41. Di Paola, M., La Mendola, L., and Navarra, G. “Stochastic seismic analysis of structures with non-linear viscous dampers”, *J. Stru. Eng.*, **133**(10), pp. 1475–1478 (2007).

42. Sundararajan, C. “An iterative method for the generation of seismic power spectral density functions”, *Nucl. Eng. Des.*, **61**(1), pp. 13–23 (1980).
43. Alembagheri, M. “Earthquake damage estimation of concrete gravity dams using linear analysis and empirical failure criteria”, *Soil Dyn. Earth. Eng.*, **90**, pp. 327–339 (2016).
44. U.S. Army Corps of Engineers (USACE), “Simplified analysis of concrete gravity dams including foundation flexibility”, Report No. 0704-0188 Washington, District of Columbia, United States (1989).
45. Joghataie, A. and Dizaji, M.S. “Reducing extent of cracks and increasing time to failure of concrete gravity dams by optimization of properties of layers of concrete”, *Scie. Ira.*, **21**(1), pp. 67–81 (2014).
46. Ghaemian, M., Vafai, A.H., and Karimi, Z. “Nonlinear seismic response of concrete gravity dams due to foundation fault movement”, *Scie. Ira.*, **21**(5), pp. 1539–1548 (2014).
47. Sotoudeh, M.A., Ghaemian, M., and Moghadam, A.S. “Determination of limit-states for near-fault seismic fragility assessment of concrete gravity dams”, *Scie. Ira.*, **98**(21), pp. 1–23 (2018).
48. Zacchei, E. and Brasil, L.R.F.R.M. “Seismic action on oil storage tanks: Induced pressures, total response and state of buckling”, *Inter. J. Mod. Sim. Petr. Indu.*, **10**(1), pp. 45–53 (2017).
49. U.S. Army Corps of Engineers (USACE) “Theoretical manual for analysis of arch dams”, Technical Report ITL-93-1, Washington, District of Columbia, United States (1993).
50. Millán, M.A., Young, Y.L., and Prévost, J.K. “The effects of reservoir geometry on the seismic response of gravity dams. Part 1: Analytical model”, *Earth. Eng. Stru. Dyn.*, **00**, pp. 1–6 (2002).
51. Comité Européen de Normalisation (CEN) “Design of structures for earthquake resistance - Part 4: Silos, tanks and pipelines”, EN 1998-4:2006, Brussels, Belgium (2006).
52. Wolfram Mathematica (Version 11 Student Edition), Wolfram Research, Inc (2017).
53. Clough, R.W. and Penzien, J., *Dynamics of Structures*, 3rd Ed., McGraw-Hill, New York (2003).

Biographies

Enrico Zacchei is a Senior Engineer and Researcher at Itecons Institute, Portugal. He received a PhD from University of Salamanca (USAL), Spain, in cooperation with University of São Paulo (USP), Brazil, in Structures; a PhD from University of São Paulo State

(UNESP) in the same field; an MS degree in Structural Engineering from University Roma Tre (Uniroma3), Italy; and a BS degree in Civil Engineering from Uniroma 3. He also received 10 disciplines as other postgraduate university studies at USP and UNESP; and 12 grants/scholarships, with three of them for stays in public R&D centres: USP (2 years), UNESP (8 months), Universidad de Malaga (9 months). He is the reviewer of WoS and Scopus journals, researcher in the group of “Dynamic Experimental Analysis of Structures” at USP, a member of the “Portuguese Society of Seismic Engineering” (SPES) at LNEC, Portugal, and of the Reviewer Board for Infrastructures Journal (WoS). He has 6-years work experience in engineering, especially in the major area of civil projects and structures, hydraulic engineering and road infrastructure. Dr. Zacchei is Structural Engineer and job leader in national and international companies. He has had 16 technical projects and 5 R&D projects funded through competitive calls of public/private entities (coordinator of 1 research project and 1 technical project). He has published more than 10 scientific papers in high impact journals (WoS and SCOPUS), and more than 25 participations/presentations/publications in international congresses.

José Luis Molina received a BSc degree in Environmental Sciences in 2002 from Granada University (Spain) and three MSc degrees in Environment and Water Management and Hydraulics. Dr. Molina obtained a PhD in Groundwater Management in 2009 from Geological Survey of Spain and Granada University. He also received a degree in Civil Engineering (Civil Construction specialty) in 2015. He has worked internationally with many research groups, Oxford University Centre for the Environment (OUCE), Land Water and Air Department at University of California-Davis, etc. He obtained a Postdoc Research Fellow Position at the Integrated Catchment Assessment and Management Centre (iCAM) of the Australian National University (ANU) in 2010. Then, he secured another Postdoc position at the Research Institute of Water Engineering and Environment (IIAMA) of the Polytechnic University of Valencia (UPV). Currently, he is an Associate Professor at the Hydraulic Engineering Area of the Land and Cartographic Engineering Department of Salamanca University. Dr. Molina has presented over 30 JCR publications in SCI high-impact research journals such as “Journal of Hydrology”, “Environmental Modelling and Software”, and “Water Resources Management”.